ISSN 1063-7826, Semiconductors, 2015, Vol. 49, No. 12, pp. 1671–1677. © Pleiades Publishing, Ltd., 2015.
Original Russian Text © I.A. Andreev, O.Yu. Serebrennikova, N.D. Il'inskaya, A.A. Pivovarova, G.G. Konovalov, E.V. Kunitsyna, V.V. Sherstnev, Yu.P. Yakovlev, 2015, published in Fizika i Tekhnika Poluprovodnikov, 2015, Vol. 49, No. 12, pp. 1720–1726.

PHYSICS OF SEMICONDUCTOR DEVICES

Photoelectric Properties of Photodiodes Based on InAs/InAsSbP Heterostructures with Photosensitive-Area Diameters of 0.1–2.0 mm

I. A. Andreev*, O. Yu. Serebrennikova, N. D. Il'inskaya, A. A. Pivovarova, G. G. Konovalov, E. V. Kunitsyna, V. V. Sherstnev, and Yu. P. Yakovlev

Ioffe Physical–Technical Institute, Russian Academy of Sciences, St. Petersburg, 194021 Russia

** e-mail: igor@iropt9.ioffe.ru*

Submitted May 12, 2015; accepted for publication May 18, 2015

Abstract—The results of a study aimed at the development of high-efficiency photodiodes for the spectral range 1.5–3.8 μm with various photosensitive-area diameters in the range 0.1–2.0 mm are reported. Epitaxial techniques for the growth of InAs/InAsSbP photodiode heterostructures are developed. The distinctive features of the diodes are their high monochromatic current sensitivity S_λ of up to 1.6 A/W at the peak of the spectrum, $\lambda = 3.0–3.4$ μm, and the detectivity of the photodiodes, estimated by the experimentally measured noise level and the monochromatic current sensitivity, reaching at the spectrum peak a value of D^* (λ^{max}, 1000, 1) = $(0.6–12) \times 10^{10}$ cm $Hz^{1/2}$ W^{-1} at $T = 300$ K. The bulk component of the reverse dark current in the photodiodes under study is constituted by two components: diffusion- and tunneling-related, with a low density of reverse dark currents $j = (0.3–6) \times 10^{-1}$ A/cm^2 attained at a bias of $U = -(0.2–0.4)$ V. The photodiodes are characterized by the product $R_0A = 0.4–3.2$ Ω cm^2. With the diameter of the photosensitive-area increased within the range 0.1–2.0 mm, the specific detectivity of a photodiode increases by nearly a factor of 2, which is due to the weaker effect of surface leakage currents with its increasing diameter. The response time of diodes of this kind varies within the range 1–300 ns, which enables their use in open-space optical communication systems in the atmospheric-transparency window. Photodiodes with a large sensitive area (up to 2.0 mm), high specific detectivity, and high photosensitivity can be used to detect absorption bands and record the concentrations of such substances as methane, ether, N_2O, and phthorothanum.

DOI: 10.1134/S1063782615120027

1. INTRODUCTION

The spectral range 1.5–4.0 μm is of particular interest for hardware engineers developing apparatus used in the laser-diode spectroscopy of gases and molecules, laser range finding and location systems, medicine, and ecological monitoring [1–4]. The main problem in all these areas lies in detecting the smallest possible optical signal. In this context, for a photodetector the main role is played by the threshold characteristics which determine the values of small optical signals that can be recorded at the noise level. To provide the minimum noise level, it is necessary for a photodiode (PD) to have a low dark current and, accordingly, high dark resistance in the case of operation in the photovoltaic mode. When a PD is used with a preamplifier to obtain a low noise level and wide bandwidth of a device, the PD should have the lowest possible capacitance. In addition, the specific detectivity grows with increasing diameter of the photosensitive area of a PD. The large sizes of photosensitive areas impose special requirements on surface uniformity and on the quality of heterointerfaces in semiconductor epitaxial structures from which PDs are fabricated.

At the Laboratory of infrared optoelectronics, Ioffe Physical–Technical Institute, effective light-emitting diodes, lasers, and PDs whose spectral sensitivity is matched with the lasers have been fabricated on the basis of multicomponent narrow-gap InAs/InAsSbP solid solutions by both liquid-phase epitaxy (LPE) and metal-organic vapor-phase epitaxy (MOVPE) [5–7]. PDs fabricated on the basis of InAs/InAsSbP heterostructures in the above-mentioned studies have rather good photoelectric characteristics, but their photosensitive areas are as small as 0.2–0.3 mm. The PDs demonstrated the following characteristics at room temperature: reverse dark currents of 200–300 μA ($U = -0.2$ V) and a detectivity of $(4–7) \times 10^9$ cm $Hz^{1/2}$ W^{-1} [5, 6]. The response time of the PDs was 10–20 ns at a photosensitive-area diameter of 300 μm. In [7], the detectivity of PDs based on an InAsSbP/InAs/InAsSbP double heterostructure reaches a value of $(1–2) \times 10^{11}$ cm $Hz^{1/2}$ W^{-1}, but this is due to the use of immersion lenses with a diameter of up to 3.3 mm. The dark currents of PDs of this kind with overall dimensions of 150 × 150 μm were 20–50 μA ($U = -0.2$ V).

The goal of our study is to develop InAs/InAsSbP heterophotodiodes with a spectral sensitivity range of

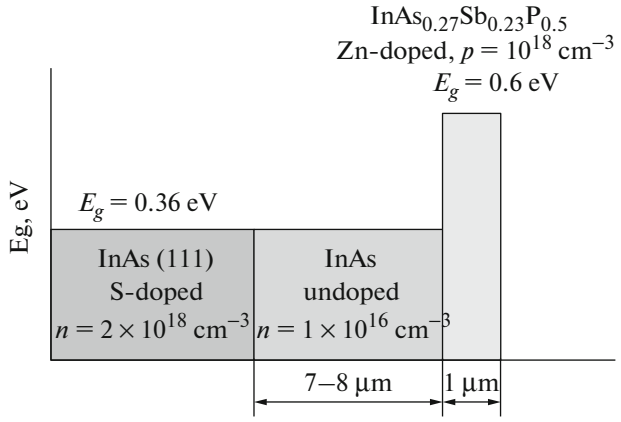

Fig. 1. Band diagram of an n^+-InAs–n^0-InAs–P^+-$InAs_{0.27}Sb_{0.23}P_{0.5}$ heterophotodiode grown by the MOVPE method.

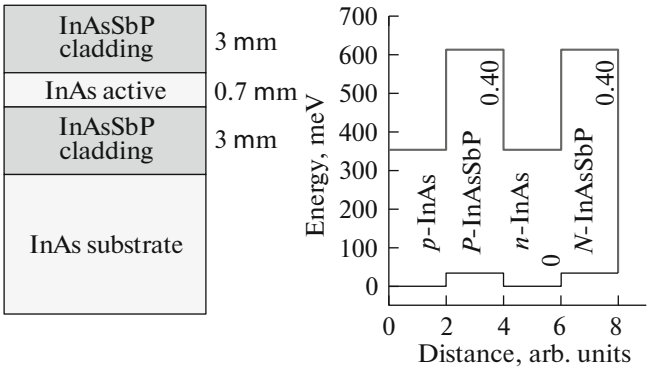

Fig. 2. Structure and band diagram of an InAsSbP/InAs/InAsSbP double heterostructure grown by the LPE method.

2.0–3.8 μm, fabricated by both the LPE and MOVPE method with various photosensitive-area diameters of 0.1–2.0 mm, and examine the photoelectric characteristics of these devices.

2. DEVELOPMENT OF LATTICE-MATCHED InAs/InAsSbP HETEROSTRUCTURES

Lattice-matched InAs/InAsSbP PD heterostructures were grown by two technological processes: MOVPE and LPE. Let us first consider vapor-phase epitaxy for the growth of InAs/InAsSbP heterostructures with a wide-gap "window," an InAsSbP layer with a high content of phosphorus, $P = 0.50$.

2.1. MOVPE Growth of InAs/InAsSbP PD Structures

The InAs/InAsSbP heterostructures were grown in a standard MOVPE reactor with horizontal gas flow, operating under atmospheric pressure. The epitaxial layers were grown on InAs substrates located on molybdenum susceptors. *n*-InAs (111) substrates doped with sulfur (S) to a carrier concentration of 2×10^{18} cm^{-3} were used. An undoped autoepitaxial *n*-type InAs layer with a thickness of 7–8 μm and concentration of 1×10^{16} cm^{-3} was situated on the substrate. The following precursors were used to grow $InAs_{0.27}Sb_{0.23}P_{0.50}$: trimethylindium (TMIn), trimethylantimony (TMSb), diethylzinc (DeZn), and also phosphine (PH_3) and arsine (AsH_3), diluted with hydrogen H_2 to 20%. Hydrogen served as the carrier gas at a flow rate of 18 L/min. $InAs_{0.27}Sb_{0.23}P_{0.50}$ was grown at a temperature of 520°C, the growth rate of the InAsSbP layer was 2 μm/h. Layers with *p*-type conduction and a concentration on the order of ~10^{18} cm^{-3} were obtained by doping with Zn by passing a H_2 flow through a DeZn bubbler at a rate of 25 mL/min. A wide-gap layer was grown with a thickness of about 1 μm. Measurements by the electron-beam-induced current (EBIC) method demonstrated that zinc diffuses from the upper wide-gap $InAs_{0.27}Sb_{0.23}P_{0.50}$ into the undoped *n*-InAs layer, thereby making a part of the InAs layer *p*-type. Thus, a *p*–*n* junction is formed in the "buffer" layer at a distance of 1.5–2.0 μm from the $InAs_{0.27}Sb_{0.23}P_{0.50}$/InAs heterointerface. The advantage of a structure of this kind is that a wide-gap $InAs_{0.27}Sb_{0.23}P_{0.50}$ layer is grown with an energy gap of about 0.6 eV, which substantially extends the spectral sensitivity range to 2.0 μm in the short-wavelength part of the spectrum. The structure is shown schematically in Fig. 1.

The lattice mismatch between the $InAs_{0.27}Sb_{0.23}P_{0.50}$ and InAs layer was found by X-ray diffraction analysis to be $\Delta a/a < 6 \times 10^{-4}$.

2.2. LPE-Grown InAs/InAsSbP PD Structures

The heterophotodiode structures were grown on *p*-InAs (100) substrates by the LPE method in the form of double heterostructures (see Fig. 2). The LPE of the structures was performed with standard horizontal multiwell graphite cassettes of the slider type. Epitaxy was carried out in a reactor with a quartz tube in a flow of hydrogen purified with a palladium filter. This yielded double heterostructures containing an *n*-type undoped active layer InAs confined between *P*- and *N*-type wide-gap InAsSbP layers with a phosphorus content of about 0.40 and an energy gap of E_g = 570 meV at T = 300 K. The width of the InAs active region was 0.7–1.0 μm. The AsSbP layers had a thickness of 3.0 μm and were lattice-matched with both the substrate and the active InAs layer. The residual carrier concentration in the active layer was reduced to 5×10^{15} cm^{-3} (T = 300 K) by gettering the solution-melt with a rare-earth element ytterbium Yb. The *N*- and *P*-type wide-gap InAsSbP layers were doped with tin (Sn) to a concentration of 5×10^{18} cm^{-3} and with zinc (Zn) to 1×10^{18} cm^{-3}, respectively.

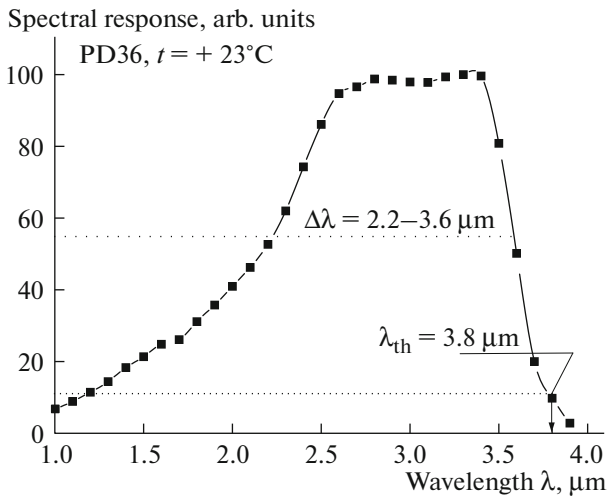

Fig. 3. Spectral distribution of the photosensitivity of an InAs/InAsSbP heterophotodiode.

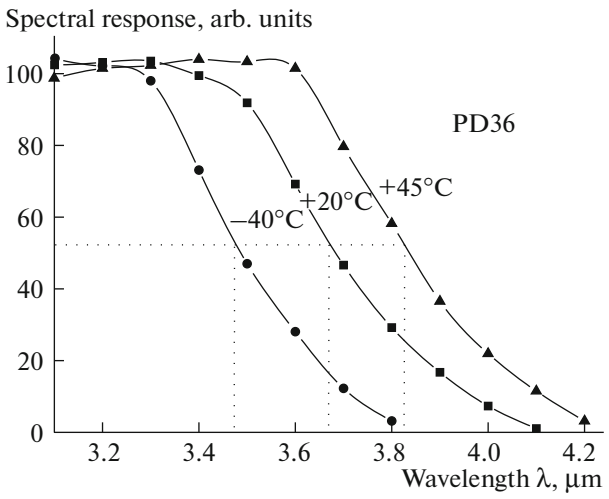

Fig. 4. Variation of the long-wavelength spectral sensitivity threshold of photodiodes based on an InAs/InAsSbP heterostructure with temperature.

The resulting heterostructures were used to fabricate mesa PDs with sensitive-area diameters in the range 0.1–2.0 mm by standard photolithography. Then, we studied in detail the basic photoelectric characteristics of InAs/InAsSbP heterophotodiodes grown by the LPE and MOVPE methods. The results we obtained are presented in the following sections of the publication. The data for PDs with sensitive-area diameters of 0.2 and 0.5 mm will be presented in most detail, with the results for PDs having other sensitive-area diameters of 0.1, 0.3, 1.0, and 2.0 mm given at the end.

3. SPECTRAL CHARACTERISTICS OF InAs/InAsSbP HETEROPHOTODIODES

It can be seen in the spectral sensitivity distribution for a typical PD (see Fig. 3) that the cutoff wavelength (at 10% of the maximum value) is 3.8 μm at room temperature. The monochromatic current sensitivity at the spectral peak (λ = 3.1–3.4 μm) was 1.4–1.6 A/W, which corresponds to a quantum efficiency of 0.5–0.6 without any antireflection coating. For the LPE-grown PDs with a double heterostructure, the monochromatic current sensitivity at the spectral peak was 1.0–1.2 A/W, which corresponds to a quantum efficiency of 0.35–0.45. One of the reasons for a possible decrease in sensitivity is that the width of the active region is only 0.7–1.0 μm, whereas calculations show that the absorption region at an absorption coefficient of 3×10^4 cm^{-1} and a wavelength of about 3 μm must be no less than 2.5–3.0 μm.

We also examined the variation in the long-wavelength part of the photosensitivity spectrum with temperature (Fig. 4). The shift of the wavelength of the absorption edge with temperature in the long-wavelength part of the spectrum at half the maximum sensitivity exhibits a linear dependence with a slope ratio of 3 nm/K, which indicates that the change in the energy-gap width with temperature is $\Delta E_g/\Delta T = 2.85 \times 10^{-4}$ eV/K ($E_g = 0.44 - 2.85 \times 10^{-4}\,\Delta t$).

4. CURRENT–VOLTAGE AND CAPACITANCE–VOLTAGE CHARACTERISTICS OF InAs/InAsSbP HETEROPHOTODIODES

There exist requirements to the reverse dark current of PDs because the detectivity is determined by the dark current I_d (PD mode) or the shunting resistance $R_0 = (dU/dI)_{U=0\text{ V}}$ (photovoltaic mode). Both the dark current and the shunting resistance strongly depend on the energy-gap width of the solid solution and on the dark-current mechanism:

$$I_d \propto \exp(-E_g/nkT), \qquad (1)$$

where n is the parameter that is determined by the nature of the dark current and varies from $n = 1$ (interband-recombination mechanism) to $n = 2$ (generation-recombination mechanism). In this context, it seemed necessary to study the nature of the dark current in InAs/InAsSbP PD heterostructures. We examined the current–voltage (I–U) characteristics of the heterophotodiodes in a wide temperature range from 77 to 330 K (–196°C...+60°C). The dependences of the reverse dark current on the reverse bias and temperature for PDs with sensitive-area diameters of 0.2 and 0.5 mm are shown in Figs. 5a and 6. Figure 5b shows the temperature dependence of the reverse current for photodiodes with a sensitive-area diameter of 0.2 mm under a bias of $U = -0.1$ V. The same figure presents the calculated run of the temperature depen-

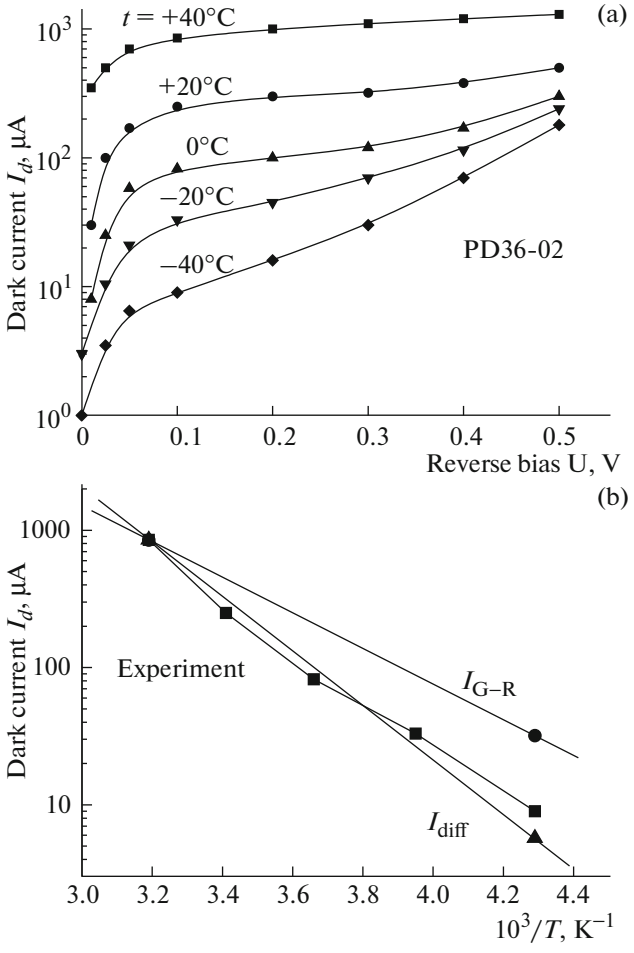

Fig. 5. (a) Dependence of the reverse dark current of a photodiode based on an InAs/InAsSbP heterostructure (diameter 0.2 mm) on bias at various temperatures. (b) Temperature dependence of the reverse dark current of the photodiodes at a fixed bias $U = -0.1$ V.

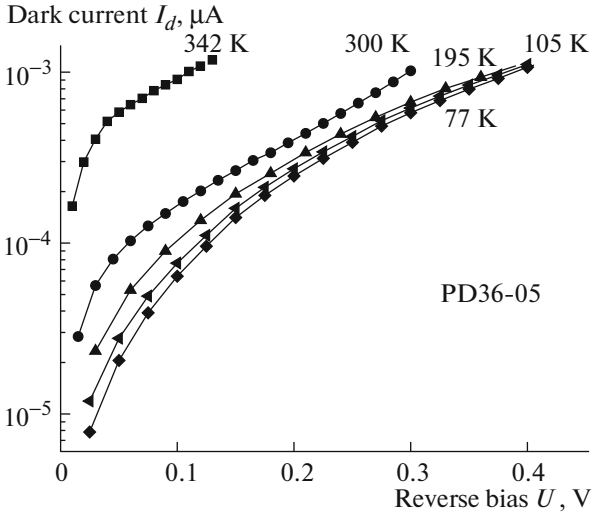

Fig. 6. Dependence of the reverse dark current of a photodiode on an InAs/InAsSbP heterostructure ($D = 0.5$ mm) on bias at various temperatures.

dences for the generation-recombination (G–R) and diffusion current mechanisms:

$$I_{G-R} \propto T^{3/2} \exp(-E_g/2kT), \quad (2)$$

$$I_{\text{diff}} \propto \exp(-E_g/kT). \quad (3)$$

Apparently, these temperature dependences best agree with the diffusion nature of the reverse dark current in the temperature range 313–233 K. Further analysis of the reverse current of InAs/InAsSbP heterophotodiodes with a sensitive-area diameter of 0.2 mm demonstrated that the dark current is constituted by two components: diffusion- and tunneling-related. At temperatures below 233 K, a deviation from the theoretical dependence is observed because the tunneling component of the dark current increases as the materials are narrow-gap and have a direct-gap structure, which gives rise to the tunneling-related component of the dark current. The same constituent is also manifested at high reverse biases because of an increase in the electric-field strength in the heterostructure, which also leads to a rise in the tunneling-related component of the reverse dark current.

At room temperature and reverse voltages higher than 0.1–0.2 V, the dependence $I(U)$ is weak ($I \propto W \propto U^{1/2}$) and described by

$$I = qn_iAW/\tau_{\text{eff}}, \quad (4)$$

where q is the elementary charge; A is the area of the p–n junction; W is the width of the space-charge region; n_i is the intrinsic concentration of carriers; and τ_{eff} is the effective lifetime of minority carriers. Using this relation and the room-temperature value of the current, we calculated τ_{eff} to be (6–7) × 10^{-6} s, in agreement with the time constant of radiative recombination in p-InAs [8]. We used in these calculations, the energy-gap width $E_g = 0.36$ eV and the intrinsic concentration in InAs, $n_i = 2.5 \times 10^{15}$ cm^{-3}. The activation energy for this temperature dependence was 0.2 eV, which is close to half the energy-gap width of the InAs material. We also estimated the reverse dark-current densities typical of PDs to be j = (0.3–6) × 10^{-1} A/cm^2. An analysis of the forward I–U characteristics demonstrated that the current is described by the dependence

$$I = I_0 \exp(qU/\beta kT), \quad (5)$$

where β is the ideality factor, which increases, as temperature is lowered, from β = 1.03 in the temperature range 340–230 K to a value of β = 4.2. This also indicates that the dark-current mechanism changes from that of the diffusion type to the tunneling-related mechanism.

We were able to find that the nature of the reverse dark current in all InAs/InAsSbP heterophotodiodes with sensitive-area diameters of 0.1 to 2.0 mm is about

Parameters of InAs/InAsSbP heterostructure photodiodes with sensitive-area diameters of 0.1–2.0 mm

Parameter	PD36–01	PD36–02	PD36–03	PD36–05	PD36–10	PD36–20
Sensitive-areadiameter D, mm	0.1	0.2	0.3	0.5	1.0	2.0
Long-wavelength spectral sensitivity threshold λ_s, μm	3.8	3.8	3.8	3.8	3.8	3.8
Spectral range $\Delta\lambda$ of maximum sensitivity, μm	2.9–3.4	2.9–3.4	2.9–3.4	2.9–3.4	2.9–3.4	2.4–3.4
Monochromatic current sensitivity at maximum S_λ, A/W	1.0–1.2	1.4–1.6	1.4–1.6	1.4–1.6	1.4–1.6	1.0–1.2
Dark current I_D, μA at $U_R = -0.2$ V	20–175	40–220	60–270	100–380	250–710	600–1400
Impedance R_0, kΩ ($U_R = 10$ mV)	1–3	0.4–1.5	0.3–1.0	0.2–0.7	0.1–0.4	0.04–0.1
Capacitance C, pF ($U_R = 0$ V, $f = 1$ MHz)	10–20	10–200	300–400	500–1100	700–1700	1400–3000
Pulse leading-edge and decay times, $t_{0.1-0.9}$, ns ($U_R = 0$ V, $R_L = 50$ Ω)	1–3	10–20	30–40	50–120	70–150	150–300
Detectivity $D^*(\lambda_p, 1000, 1)$, cm $Hz^{1/2}/W$	(0.3–0.6) × 10^{10}	(0.6–0.8) × 10^{10}	(0.6–1.0) × 10^{10}	(0.7–1.1) × 10^{10}	(0.6–1.2) × 10^{10}	(0.7–1.0) × 10^{10}

the same: at low reverse biases the dark current is of diffusion nature. At higher reverse biases, the reverse dark current is determined by the tunneling-related mechanism, which demonstrates a strong increase in the dark current and its weak temperature dependence.

To provide the minimum noise level, it is necessary that the photodiode should have a low reverse dark current or, accordingly, a high dark resistance at zero bias in the case of operation in the photovoltaic mode.

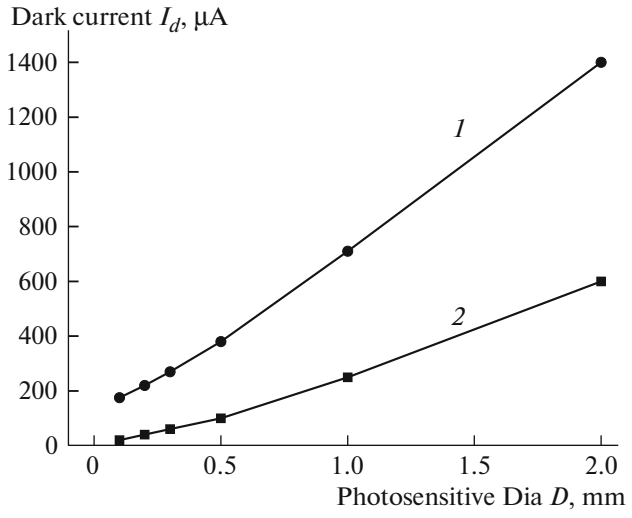

Fig. 7. Dependence of the reverse dark current of photodiodes on the photosensitive-area diameter at reverse bias $U = -0.2$ V: (*1*) maximum and (*2*) minimum currents for each diameter.

The problem of lowering the reverse dark current is closely associated with that of increasing the value of R_0. The product of the differential resistance at zero bias, R_0, by the photodiode area A, i.e., R_0A, should be as large as possible for the photodetector operating in the photovoltaic mode, when $R_0 = (dI/dU)^{-1}$ at $U = +10$ mV... -10 mV. We found for typical PDs the product $R_0A = 0.4–3.2$ Ω cm^2. The values of R_0 and the reverse dark current for heterophotodiodes with various diameters are listed in the table. Figure 7 shows how the reverse dark current depends on the photosensitive-area diameter of the heterophotodiode at a given reverse bias $U = -0.2$ V. The dependence of R_0 on diameter for the InAs/InAsSbP heterostructure with diameters of 0.1–2.0 mm is shown in Fig. 8. The maximum value of the differential resistance at zero bias, R_0, and the minimum reverse dark current are observed for photodiodes with an area of 0.1 mm. Photodiodes of this kind are fabricated with a small diameter to reduce the capacitance because it is the capacitance that is the key factor for attaining the maximum operation speed or obtaining a wider bandwidth of the photodiodes.

Measurements of the capacitance–voltage (C–U) characteristics demonstrated that the impurity distribution in all kinds of PDs is sharp and the carrier concentration in the active region is low for the InAs/InAsSbP heterostructure, $n = (0.7–1.5) \times 10^{16}$ cm^{-3}. The dependences of the capacitance on reverse bias for photodiodes with area diameters of 0.2 and 0.5 mm are shown in Fig. 9. The capacitance of the photodiodes with various diameters of 0.1–2.0 mm are presented in the table and vary from 15 to

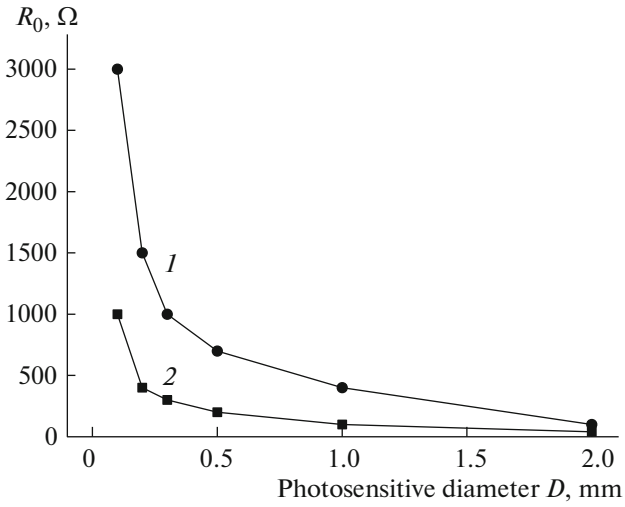

Fig. 8. Dependence of the differential resistance at zero bias, R_0, on the photosensitive-area diameter: (*1*) maximum and (*2*) minimum resistances for each diameter.

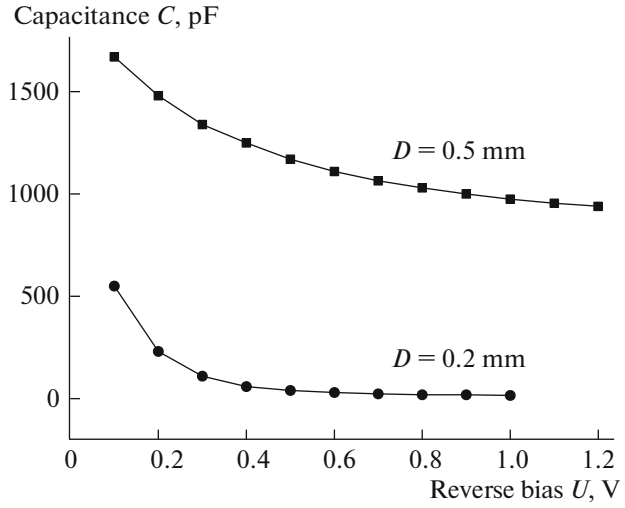

Fig. 9. Dependence of the capacitance of a photodiode based on an InAs/InAsSbP heterostructure on the reverse bias at photosensitive-area diameters of 0.2 and 0.5 mm.

3000 pF at zero bias. The capacitance of a photodiode is an important parameter determining the operation speed of a device. It was found for the structures grown by MOVPE that the response time of a photodiode is also determined by the time in which photogenerated carriers diffuse to the region of the *p–n* junction. This time is on the order of 10–15 ns. For heterophotodiodes grown by the LPE method, the response time is determined only by the *RC* component because the heterointerface coincides with the position of the *p–n* junction and carriers are immediately separated by an electric field. At a load of 50 Ω, the range of response times of the photodiodes under pulsed exposure varied within the range 1–300 ns. These times take into account both the capacitance of the photodiode (the larger its area, the higher its capacitance) and the interior position of the *p–n* junction relative to the heterointerface.

The problem of the development of fast IR photodetectors which operate at room temperature forces researchers to find new alternative approaches to the operation and design principles of the devices. The efficiency of photodiodes can be improved by raising the detectivity and the operation speed. The detectivity D^* of a photodiode is given by the following formula [9]:

$$D^* = S_i A^{1/2}/i_n, \quad (6)$$

where S_i is the monochromatic current sensitivity in A/W; A is the sensitive area in cm^2; and i_n is the noise current in A.

It follows from formula (6) that, to raise the detectivity of a photodiode, it is necessary to reduce the noise current, which is related to the reverse dark current by

$$i_n = (1qI_d\Delta f)^{1/2}, \quad (7)$$

or to reduce the noise current related to the dark resistance at zero bias by

$$i_n = (4kT\Delta f/R_0)^{1/2}. \quad (8)$$

Here, I_d is the reverse dark current in A; q is the elementary charge in C; Δf is the bandwidth of the photodetector in Hz; k is the Boltzmann constant; T is temperature in K; and R_0 is the dark resistance at zero bias in Ω. At the same time, it is necessary to make increase the sensitive area in order to raise the D^* of a photodiode. The parameters of photodiodes with various illumination-active areas are listed in the table. It is noteworthy that there are diodes with a wide variety of areas and corresponding application purposes and photodiodes of this kind have excellent sensitivity, detectivity, and operation speed.

5. CONCLUSIONS

(i) Epitaxial InAs/InAsSbP photodiode heterostructures were grown by liquid-phase epitaxy and metal-organic vapor-phase epitaxy. Photodiodes with various photosensitive-area diameters in the range from 0.1 to 2.0 mm were fabricated from these heterostructures.

(ii) The room-temperature spectral sensitivity range of the InAs/InAsSbP heterophotodiodes is 1.5–3.8 μm at a level of 10% of the spectral peak. The photosensitivity of the photodiodes at the spectral peak (λ = 3.0–3.4 μm) reached a value of S_λ = 1.6 A/W. The detectivity of the photodiodes attains at the spectral peak a value of $D^*(\lambda_{max}, 1000, 1) = (0.6–1.2) \times 10^{10}$ cm Hz$^{1/2}$ W^{-1} at T = 300 K. With the photosensitive-area diameter increasing within the range 0.1–2.0 mm,

the specific detectivity of the photodiodes nearly doubles, which is due to the decreasing effect of surface leakage current with increasing photosensitive-area diameter.

(iii) A study of the nature of the dark current in relation to the reverse bias and temperature demonstrated that the bulk constituent of the reverse dark current consists of two components: diffusion- and tunneling-related. At temperatures below 233 K and also at reverse biases higher than 0.4 V, an increase is observed in the tunneling component of the dark current. The reverse dark-current density at a bias of $U = -(0.2–0.4)$ V for the best photodiodes attains $j = (0.3–6) \times 10^{-1}$ A/cm^2, with the R_0A product of 0.4–3.2 Ω cm^2.

(iv) With the photosensitive-area diameter increasing within the range 0.1–2.0 mm, the reverse dark current also increases from 20 to 600 μA at $U = -(0.2–0.4)$ V. The capacitance of a photodiode also increases from 15 to 3000 pF, which results in a sharp decrease (by a factor of 30–50) in the operation speed of the photodiode, determined by the *RC* component. The response time of photodiodes of this kind varies within the range 5–300 ns, which, taken together with the low capacitance, enables their use in open-space optical communication systems in the atmospheric-transparency window.

(v) Photodiodes with a large sensitive area (up to 2.0 mm in diameter) and high specific detectivity can be used to find absorption bands and record the concentrations of such substances as methane (3.25, 3.31, 3.54 μm) [8], ether (λ = 1.72, 2.28, 2.9 μm), N_2O (λ = 2.85, 2.96 μm), and phthorothanum used in medicine for general anesthesia (λ = 3.32 μm).

REFERENCES

1. E. V. Stepanov, *Diode Laser Spectroscopy and Molecular Analysis of Biomarkers* (Fizmatlit, Moscow, 2009) [in Russian].
2. K. Kincade, Laser Focus World **12**, 69 (2003).
3. M. P. Mikhailova, N. D. Stoyanov, I. A. Andreev, B. Zhurtanov, S. S. Kizhaev, E. V. Kunitsyna, K. Salikhov, and Yu. P. Yakovlev, Proc. SPIE **6585**, 658526-1 (2007).
4. T. L. Troy and S. N. Thennadil, J. Biomed. Opt. **6**, 167 (2001).
5. I. A. Andreev, S. S. Kizhaev, S. S. Molchanov, N. D. Stoyanov, and Yu. P. Yakovlev, in *Proceedings of the 6th International Conference on the Mid-Infrared Optoelectronics: Materials and Devices (MIOMD), St. Petersburg, Russia, June 28–July 1, 2004,* p. 70.
6. M. Ahmetoglu (Afrailov), I. A. Andreev, E. V. Kunitsyna, K. D. Moiseev, M. P. Mikhailova, and Yu. P. Yakovlev, Infrared Phys. Technol. **55**, 15 (2012).
7. P. N. Brunkov, N. D. Il'inskaya, S. A. Karandashev, A. A. Lavrov, B. A. Matveev, M. A. Remennyi, N. M. Stus', and A. A. Usikova, Infrared Phys. Technol. **64**, 62 (2014).
8. M. Levinshtein, S. Rumyantsev, and M. Shur, in *Handbook Series on Semiconductor Parameters, Ternary and Quaternary A3B5 Semiconductors* (World Scientific, London, 1999), Vol. 2.
9. R. C. Jones, *Advances in Electronics* (New York, Academic, 1953), Vol. 5, p. 1.

Translated by M. Tagirdzhanov